nature physics

Article

https://doi.org/10.1038/s41567-023-01988-7

The hidden hierarchical nature of soft particulate gels

Received: 2 June 2022

Accepted: 7 February 2023

Check for updates

Minaspi Bantawa[1], Bavand Keshavarz[2], Michela Geri[2], Mehdi Bouzid[3], Thibaut Divoux[4], Gareth H. McKinley[2] & Emanuela Del Gado[1]

Soft particulate gels are composed of a small amount of particulate matter dispersed in a continuous fluid phase. The solid components assemble to form a porous matrix, providing rigidity and control of the mechanical response, despite being the minority constituent. The rheological response and gel elasticity are direct functions of the particle volume fraction. However, the diverse range of different functional dependencies reported experimentally has challenged efforts to identify general scaling laws. Here we reveal a hidden hierarchical organization of fractal elements that controls the viscoelastic spectrum, and which is associated with the spatial heterogeneity of the solid matrix topology. The fractal elements form the foundations of a viscoelastic master curve, constructed using large-scale three-dimensional (3D) microscopic simulations of model gels, which can be described by a recursive rheological ladder model over a range of particle volume fractions and gelation rates. The hierarchy of the fractal elements provides the missing general framework required to predict the gel elasticity and the linear viscoelastic response of these complex materials.

Soft particulate gels include materials we can eat, squeeze or 3D print, from foods to bio-inks to cement hydrates. For gels formed through polymerization reactions or crosslinking of polymers in solution, 80 years of polymer physics have provided the basis to fully understand the links between chemical architectures and rheology[1,2]. Percolation theory has been central for understanding the gel properties as a function of the distance from a gelation (percolation) threshold[3]. The self-similarity of the chemical architectures close to the percolation threshold naturally produces a hierarchy of lengthscales and timescales, leading to power-law characteristics in the viscoelastic response[4–8]. By contrast, in particulate gels, the link between microstructure and viscoelasticity remains elusive. Such gels can be formed from both synthetic or natural constituents, and represent a preferred strategy to incorporate high-value functional components while limiting costs and risks. These gels form through physical association of the initial colloidal building blocks, due to surface forces and attractive interactions mediated by the solvent[9–13]. Ultimately, they develop as non-equilibrium structures produced by frustration in the growth of aggregates, interconnected and locked into larger-scale disordered assemblies, from which rigidity and viscoelasticity emerge. There is growing evidence that in this class of gels a percolation threshold may also universally control the onset of rigidity (rigidity percolation) and gel elasticity[14–16]. However, the microscopic origins of that percolation transition and of the resulting power-law rheological response, observed over a range of compositions and solid contents, remain unclear. The extreme variability of gel microstructures[11,13,15,17] and microscopic dynamics[18–22] revealed by experiments seems to suggest that the microscopic physical origins of the macroscopic rheological response need to be established on a case-by-case basis. The particle volume fraction ϕ is the main control parameter in experiments, which invariably report a strongly varying shear modulus $G_0 \propto \phi^{f_{obs}}$; however, the observed scaling exponent f_{obs} ranges widely from 3 to 8, again questioning the existence of any universal behaviour and of a general framework to predict the mechanical response[10,23–33].

[1]Department of Physics, Institute for Soft Matter Synthesis and Metrology, Georgetown University, Washington, DC, USA. [2]Department of Mechanical Engineering, Massachusetts Institute of Technology, Cambridge, MA, USA. [3]Univ. Grenoble Alpes, CNRS, Grenoble INP, 3SR, Grenoble, France. [4]ENSL, CNRS, Laboratoire de physique, Lyon, France. e-mail: ed610@georgetown.edu

https://doi.org/10.1038/s41567-023-01988-7

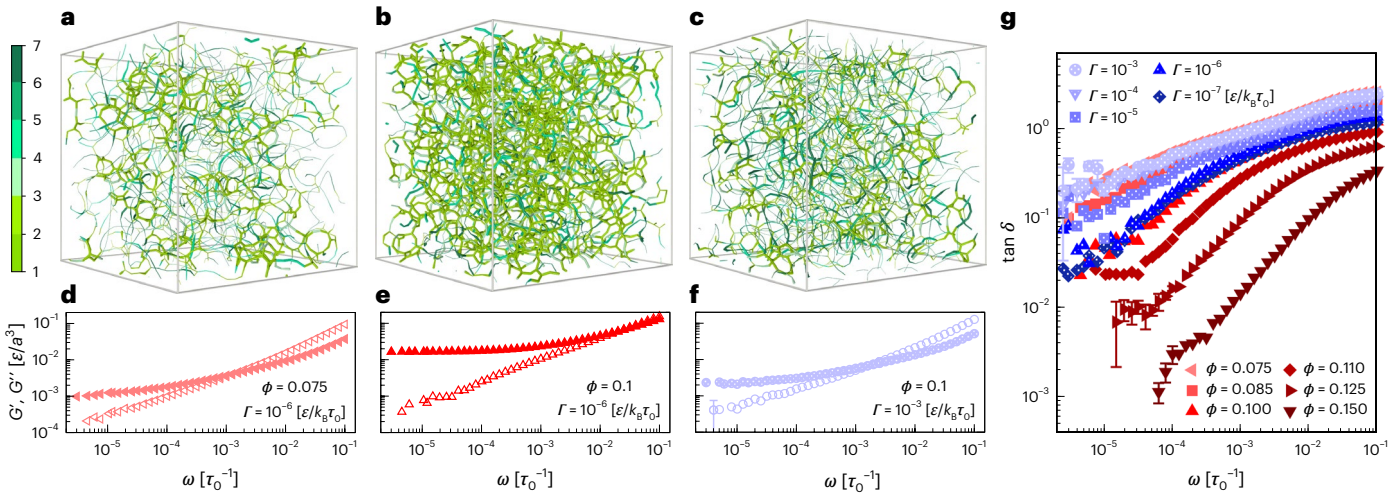

Fig. 1 | Microstructural and viscoelastic properties of networks having different connectivity. a–**c**, Simulation snapshots of gel bond networks at different particle volume fractions $\phi = 0.075$ (**a**) and $\phi = 0.1$ (**b**) prepared with a fixed gelation rate $\Gamma = 10^{-6}\,\varepsilon/k_B\tau_0$, and $\phi = 0.1$ with $\Gamma = 10^{-3}\,\varepsilon/k_B\tau_0$ (**c**). The snapshots are coloured (see scale bar) based on the mesh size, that is, on the topological distance (in units of the particle diameter) between branching points, and the thickness of the bonds is proportional to the local density of branching points. **d**–**f**, Viscoelastic moduli corresponding to **a**–**c**, where the filled and open symbols represent the storage modulus G' and loss modulus G'', respectively. **g**, Variation in the loss tangent ($\tan\delta = G''/G'$) versus frequency for gels with different volume fractions ϕ and gelation rates Γ. Typical error bars obtained from sample-to-sample fluctuations are shown for selected datasets for clarity.

Gel microstructures and rheological master curve

We use 3D numerical simulations of a particle-based model that capture the microscopic dynamics and rheology of soft particulate gels[34–38] (Methods). In terms of general trends, for a given gelation rate Γ, increasing the solid volume fraction ϕ increases, on average, the local connectivity and gel elasticity, by increasing the amount of branching in the gel (Fig. 1a,b). For a given ϕ, reducing the gelation rate also favours the branching of strands as the network self-assembles, leading to structures with higher local connectivity and elasticity (Fig. 1b,c). However, gels formed at lower ϕ are more sparsely connected, and their local connectivity is also more spatially heterogeneous (Fig. 1a).

For all gels, the linear viscoelastic spectra $G'(\omega)$ and $G''(\omega)$ (Fig. 1d–f) are computed using the OWCh protocol[37,39], which yields fast and accurate estimates of the mechanical properties over a wide range of deformation frequencies, and we use reduced simulation units to scale both moduli and frequency (Methods). As in experiments[20,27,28,40–42], varying the particle volume fractions ϕ over a relatively small range (that is, between 5% and 15%) produces apparently minor changes in the microstructure but translates into dramatic variations of the viscoelastic strength and characteristic timescales (Fig. 1d,e). Changing the gelation rate for a fixed ϕ leads to similar observations (Fig. 1e,f and Supplementary Fig. 1).

The frequency dependence of the loss tangent $\tan\delta = G''/G'$ (Fig. 1g) summarizes the mechanical response of 11 gels, obtained for different ϕ and Γ. In spite of the wide range of driving frequencies, all of the datasets are broadly self-similar and slowly approach a high-frequency plateau. A horizontal shift, rescaling the frequency either by a factor a_ϕ at a given Γ, or by a factor a_Γ at fixed ϕ, leads to a unique master curve for $\tan\delta$, covering six decades of rescaled frequency (Fig. 2a). As the reference conditions for collapsing the data, we use a volume fraction of $\phi = 15\%$ and a gelation rate $\Gamma = 10^{-6}\,\varepsilon/k_B\tau_0$, where ε is the unit energy, so that the reduced dimensionless temperature is k_BT/ε and τ_0 sets the timescale in the simulations (see Methods).

Ladder and fractional models

The resulting master curve exhibits an extended power-law regime, highlighting a hierarchy of timescales that is captured by recursively combining viscoelastic elements in a hierarchical ladder structure[43,44]. The ladder-like arrangement, sketched as an inset in Fig. 2a, comprises n viscoelastic elements with model contributions $(\tilde{E}_i, \tilde{\eta}_i)$ (with $0 \le i \le n$) and an exponent α that sets the relationship between $(\tilde{E}_i, \tilde{\eta}_i)$ and $(\tilde{E}_0, \tilde{\eta}_0)$ (equation (10) in the Methods). For large n ($n \ge 150$), the ladder model predicts a loss factor $\tan\delta$ that smoothly transitions from a linear increase to a plateau at high frequencies (Methods), in good agreement with the master curve obtained from the simulation data (Fig. 2a).

We can now vertically rescale the loss and storage moduli by a factor b_ϕ (or b_Γ) to obtain master curves for G' and G'', as shown in Fig. 2b. Taking the continuous limit of the ladder model introduced in Fig. 2a, we obtain a more compact description of the viscoelastic response in terms of a fractional Kelvin–Voigt model characterized by just four parameters: a spring constant (G_0), a viscous dashpot (η) and a fractional element or 'spring-pot' (characterized by a scale factor $\mathbb{V}$ and an exponent α)[45]. The power-law exponent $0 \le \alpha \le 1$ reflects the recursive nature of the underlying ladder model, and we can relate the other parameters to the rungs of the ladder model in the limit $n \to \infty$ (Supplementary Sections 2 and 3):

$$G_0 = \frac{\tilde{E}_0}{n^{2\alpha}},\ \eta = n^{2-2\alpha}\tilde{\eta}_0,\ \mathbb{V} = \tilde{E}_0\left(\frac{\tilde{\eta}_0}{\tilde{E}_0}\right)^{\alpha}. \qquad (1)$$

The extended power-law regime evident in the master curves and its description by a ladder model reflect the scale-free characteristics of the relaxation spectra underpinning the viscoelastic response. For polymer gels, power-law characteristics and rheological ladder models directly stem from the self-similar chemical architecture close to percolation[4,46–48]. In soft particulate gels, instead, the microstructures are often not self-similar[10,11,15,17,20], as is also the case here (Supplementary Fig. 3). Moreover, both ϕ and Γ determine the range of frequencies and viscoelasticity relevant to the power-law region of the spectra (Supplementary Fig. 1c), demonstrating the intricate coupling between particle volume fraction and gelation kinetics, which makes the microstructural origin of the rheology of this class of gels so difficult to pin down.

Lengthscale and fractal characteristics

To tease out the microscopic origin of the rheological response, we analyse the fluctuations in the spontaneous microscopic dynamics across all our gels, at rest and subjected only to thermal fluctuations

https://doi.org/10.1038/s41567-023-01988-7

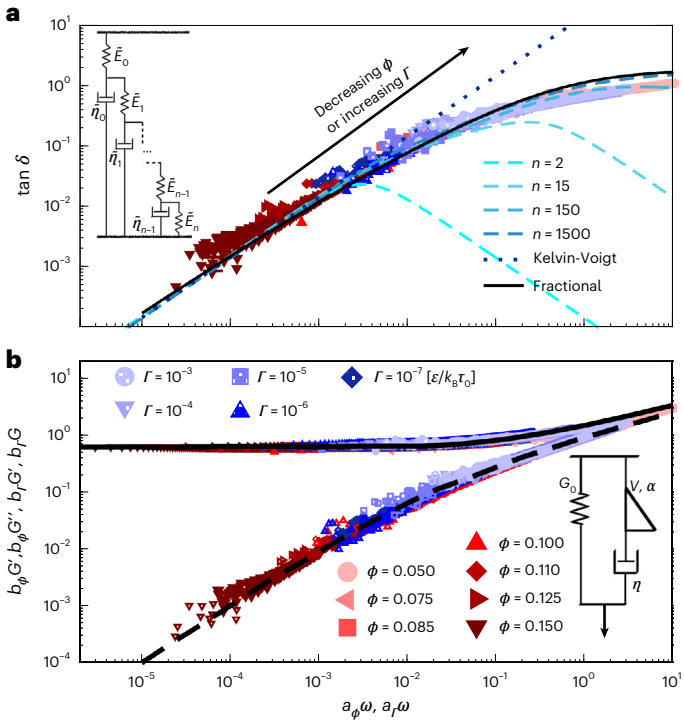

Fig. 2 | Rheological master curves and constitutive model for particulate gels. a, Superposition of the self-similar curves of tan δ onto a single master curve achieved by rescaling the imposed deformation frequency with a shift factor a_ϕ or a_Γ with respect to a reference gel at a volume fraction of $\phi = 0.15$. The functional form of tan δ predicted by ladder models with increasing number of elements n, each having spring constant E_i and viscosity η_i, as well as by the asymptotic fractional model, is shown by different lines, as listed in the legend. Inset: schematic representation of the corresponding ladder model. **b**, Master curves for the moduli with the same horizontal shift factors a_ϕ or a_Γ (in units of time τ_0) and vertical shift factors b_ϕ or b_Γ (with units inverse of the moduli). The solid and dashed lines represent, respectively, the predictions for G'' and G' with the four-parameter fractional model shown in the inset.

(Methods). In the simulations we can use a suitable range of thermal fluctuations such that no substantial changes in the gel structures are induced over the simulation time window. We then compute the displacements $\mathbf{\Delta} = \mathbf{r}(t_0 + t_w) - \mathbf{r}(t_0)$ from the particle trajectories $\mathbf{r}(t) \equiv (x(t), y(t), z(t))$, where the time interval $[t_0, t_0 + t_w]$ is such that both t_0 and t_w are in the plateau region of the particle mean-squared displacement as a function of time (Methods and Supplementary Fig. 4a). The fluctuations $u = [(\mathbf{\Delta} - \langle\mathbf{\Delta}\rangle)^2]^{1/2}$ are widely distributed across the different gel microstructures (Supplementary Fig. 4b). In complex gel architectures, both the microscopic dynamics and the mechanics are largely controlled by the presence of more densely connected regions interspersed with sparsely connected ones[36,49–52]. We therefore measure, along network strands, the distribution of topological distances l, which separate two connected branching points. This distribution provides direct access to the structural and micromechanical heterogeneities in the gels that determine floppy modes and low-frequency elasticity[53]. From the probability distribution $p(l)$ across all gels (Supplementary Fig. 5a), we extract the variance and use $\xi = \langle(l - \langle l\rangle)^2\rangle^{1/2}$, with dimensions of length, to characterize the gel mesh size heterogeneity. By rescaling all fluctuations u of the microscopic displacements with ξ^2/l_p, where l_p denotes the persistence length of the gel strands[38], the distributions $p(u)$ collected across all gels collapse onto a unique curve (Fig. 3a). Hence the variation of ξ with ϕ and Γ captures the microstructural origin of the variations in the microscopic dynamics.

As the gels become softer with decreasing ϕ or increasing Γ, less-connected networks are produced, and ξ grows because less-connected networks are also more spatially heterogeneous. Extrapolating, at the very onset of rigidity, ξ captures the first rigid backbone, a single branch that spans the whole gel and that is sufficient, alone, to provide rigidity. These considerations point to ξ as a direct probe of the distance from the rigidity threshold in our gels. Such a metric, in fact, is ultimately set by the number of branching points, which we can measure, in our model gels, through the volume fraction ϕ_{br} of particles with coordination $z = 3$. Although ξ varies with both ϕ and Γ, the data across all gels follow the scaling $\xi \propto \phi_{br}^{-\nu}$ (Fig. 3c), suggesting that indeed ξ may capture the scaling of the critical correlation length associated with the rigidity transition that governs the emerging gel elasticity. The computed estimate for $\nu \simeq 0.80 \pm 0.16$ is compatible with the value of a 3D random percolation network[48]. Since we verify from the plateau in G' at low frequencies that all our gels are rigid, the power-law dependence of ξ on ϕ_{br} may reflect that, because of their extreme softness and structural complexity, soft particulate gels are marginally rigid and remain relatively close to a rigidity percolation threshold over a range of particle volume fractions.

If the rigidity percolation transition in particulate gels is akin to a random percolation, then following the blob–links–nodes model for the self-similar structure of a spanning cluster in percolation theory[46,48,54], each particulate gel is, effectively, a disordered network composed of fractal elements (blobs) whose linear size scales with ξ and whose fractal dimension is d_f. For a gel sample of linear size L, the volume L^d (in d dimensions) will consist of $(L/\xi)^d$ sub-boxes, each containing a mass fraction of the gel that is $\propto \xi^{d_f}$. Close to the percolation threshold, the scaling hypothesis for a critical point dictates that $M(L, \xi) \propto \xi^{d_f} m(L/\xi)$, where the scaling function is $m(L/\xi) = (L/\xi)^{d-d_f}$ (ref. 48).

When we compute the gel mass for samples with a range of sizes L for each volume fraction (here L is the linear size of the simulation box), the data are spread out and grow as L^3 (inset, Fig. 3b). However, if we use the scaling argument just laid out, all data collapse onto the unique scaling function $m(L/\xi)$ developed above (Fig. 3b) for $d_f \simeq 2.46 \pm 0.12$, a fractal dimension again consistent with a 3D random percolation network (Supplementary Fig. 7b). Inferring the frequency dependence of the viscoelastic modulus just from d_f as $\alpha = d/(d_f + 2)$, as proposed for polymer networks[6,21,22], yields $\alpha \simeq 0.67$ in good agreement with the predictions of the fractional and ladder models ($\alpha = 0.66 \pm 0.05$) for the viscoelastic master curves (Fig. 2a,b).

Following further the blob–links–nodes model, each fractal element should contain loops and *singly connected bonds*, whose number N_{SCB} diverges, as ξ also does, at the percolation threshold ($N_{SCB} \propto \xi^{1/\nu}$). Indeed, close enough to the threshold, singly connected bonds should be present at all lengthscales, and organized in a self-similar fashion[54]. This implies that $N_{SCB} \propto 1/\phi_{br}$, and that ϕ_{br} contains the information on how singly connected bonds become progressively more prevalent, over all lengthscales, as $\xi \longrightarrow L$ (and $\phi_{br} \longrightarrow 0$). Hence the fact that ξ and ϕ_{br} control both the microscopic dynamics and the bulk rheology of our gels can be directly related to the hierarchical organization of the singly connected structures.

The fractal blobs whose linear size $\propto \xi$ and with fractal dimension d_f fill the gel volume for any $\phi_{br} \neq 0$, hence $\xi \propto \phi^{-1/(d-d_f)}$ and, combining with $\xi \propto \phi_{br}^{-\nu}$, we obtain $\phi_{br} \propto \phi^{1/\nu(d-d_f)}$. The simulation results satisfy this scaling prediction, if we use $\nu \simeq 0.8$ and $d_f \simeq 2.5$ as obtained previously from our data (Fig. 3d). We note that, if these fractal elements controlling the rheology were the fractal aggregates formed through diffusion-limited or reaction-limited cluster aggregation (respectively DLCA or RLCA), quite common in colloidal suspensions, their fractal dimensions would be different (respectively $d_f \approx 1.8$ or $d_f \approx 2.1$; refs. 9,23,55) and this would lead to markedly different scalings between ϕ_{br} and ϕ (cf. Fig. 3d). For DLCA aggregates our scaling translates into $\phi \propto \phi_{br}$, with the particle volume fraction directly setting the distance from the rigidity threshold, consistent with the analysis of fractal aggregation in colloidal gels[9,56]. The aggregation process considered

https://doi.org/10.1038/s41567-023-01988-7

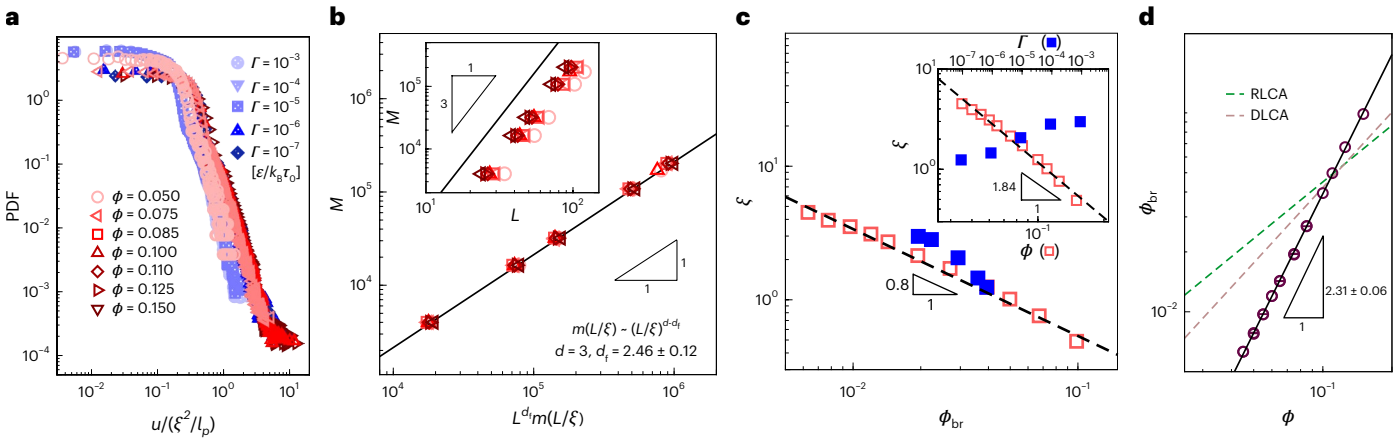

Fig. 3 | Structural characterization of gel networks. a, Distributions of fluctuations of displacements $u = [(\boldsymbol{\Delta} - \langle\boldsymbol{\Delta}\rangle)^2]^{1/2}$ normalized by ξ^2/l_p. The data refer to samples with 10^5 particles. **b**, Master curve for the mass M (made dimensionless with the particle mass) of the gel network versus normalized system size $L^{d_f} m(L/\xi)$ for different volume fractions, where $m(L/\xi) = (L/\xi)^{d-d_f}$ with a fractal dimension $d_f = 2.46 \pm 0.12$. The data are obtained by changing the system size for different volume fractions (the symbols are the same as in **a**). Inset: M versus system size L. **c**, Correlation length $\xi = \langle(l - \langle l\rangle)^2\rangle^{1/2}$ (in units of the particle diameter). The open (resp. filled) squares correspond to various volume fractions ϕ (resp. gelation rate Γ). The dashed line is a power law of exponent −0.8. Inset: evolution in correlation length ξ versus volume fraction ϕ (bottom axis and open squares) and versus gelation rate (top axis and filled squares). **d**, Volume fraction of branching points ϕ_{br} versus the volume fraction of particles ϕ: circles correspond to the simulations data. The continuous line shows the best fit of the data by a power law of exponent 2.31 ± 0.06. Corresponding predictions for the DLCA and RLCA scenarios are shown by dashed lines of slope 1.00 ± 0.06 and 1.30 ± 0.06, respectively.

here corresponds to a more general case, as density fluctuations and collective microscopic dynamics contribute to the microstructure development[14], and may apply, at a coarse-grained level, to a broader range of particulate gels[11,15,29,53].

Elastic percolating network

We now consider the mechanics of fractal elements of linear size $\propto \xi$ having elastic stiffness K_ξ. Assuming that they are uniformly distributed in space, the resulting elastic stiffness of the gel can be estimated as $K \propto (L/\xi)^{d-2} K_\xi$. With bending elasticity[57], K_ξ directly depends on the presence of singly connected bonds $K_\xi = K_0/(N_{SCB}\xi^2)$, where K_0 is the torsional bending stiffness between neighbouring bonds, which, in our case, can be computed from the microscopic interactions[38]. Identifying the rigidity transition with random percolation as demonstrated above, close enough to the threshold, the gel modulus G_0 should scale with ξ as

$$G_0 \propto \xi^{-f/\nu}, \tag{2}$$

where $f = \nu d + 1$ (ref. 57). Based on Fig. 3 and the related discussion, these theoretical scaling predictions imply that $G_0 \propto \phi_{br}^f$. For $\nu \simeq 0.8$ we find that $f \simeq 3.5$ in 3D. The scaling that we measure as a function of ϕ_{br} (or ξ) from the low-frequency shear modulus G_0 of our gels, which also coincides with the vertical shift factor b in our master curves (Supplementary Fig. 8), matches well with this prediction ($f = 3.55 \pm 0.04$) (Fig. 4a). We note that, in the case of DLCA aggregates constituting the fractal elements responsible for rigidity, since $\phi \propto \phi_{br}$ (Fig. 3d), we obtain $G_0 \propto \phi^f$ and $f \simeq 3.5$, in agreement with the behaviour typically found in colloidal gels where diffusion-limited aggregation processes form the initial fractal flocs[23,56]. Our analysis therefore highlights how the dependence of ϕ_{br} (which measures the distance from the rigidity threshold) on ϕ (the actual particle content) changes with the specific aggregation process at play (see three examples in Fig. 3d). In experiments, however, typically only ϕ is directly controllable, from which a general dependence $G_0 \propto \phi^{f_{obs}}$ can be extracted. Hence, while the rigidity percolation transition remains universal to particulate gels, we obtain

$$f_{obs} = f/\nu(d - d_f), \tag{3}$$

which naturally has a range of values depending on the fractal dimension of the gel, d_f (as reflected in Table 1), shedding light onto a wide range of experimental observations[10,23,24,26–32,58] (Supplementary Information).

Finally, the horizontal shift factors in our master curves (Fig. 2b,c) identify a characteristic timescale τ that we can trace back to the delay time for the gel elastic response to emerge from the microscopic fluctuations (Supplementary Fig. 8), which follows the same scaling as the elastic modulus G_0. This result, which can be tested in microrheology experiments, explains why the viscous element of the fractional model remains essentially constant for all of the gels (Fig. 4a). The scaling of τ with the critical lengthscale $\propto \xi$ that describes the fractal blobs (and ϕ_{br}) is yet another strong signature of how the topology dependence of the gel modulus and heterogeneity determine the relaxation spectra.

From fractal characteristics to a hierarchical ladder model

We now demonstrate that the fractal blobs, uniformly distributed in d dimensions, indeed give rise to a mechanical ladder model (Fig. 4b), as hypothesized in Fig. 2. This model results in a compact description characterized by the four microscopic parameters E_0, η_0, n and α, and the overall mechanical response can be obtained as

$$(\tilde{E}_0, \tilde{\eta}_0, \tilde{\mathbb{V}}) = \left(\frac{L}{\xi}\right)^{d-2} (E_0, \eta_0, \mathbb{V}), \tag{4}$$

where $(L/\xi)^{d-2}$ is a purely geometrical factor. The elasticity of the ladder structures is set by the bending stiffness of the gel strands $E_0 \propto K_0/a^3$, where K_0 is the torsional stiffness, with dimension of [force × length], and a is the unit distance between neighbouring particles in our simulations. By combining the expressions for the overall elastic modulus of the ladder model (G_0) as a function of the number n of elements in each ladder structure (equations (1) and (4)), we find that G_0 is related to the torsional stiffness K_0 through a structure-dependent factor $G_0 \propto (L/\xi)^{d-2} K_0/(a^3 n^{2\alpha})$. Similarly, in disordered elastic networks with bending elasticity[57], the scaling $G_0 \propto (L/\xi)^{d-2} K_\xi/L$ implies that $G_0 \propto (L/\xi)^{d-2} K_0 N_{SCB}^{-2\nu-1} a^{-2}/L$. These two distinct scaling expressions

https://doi.org/10.1038/s41567-023-01988-7

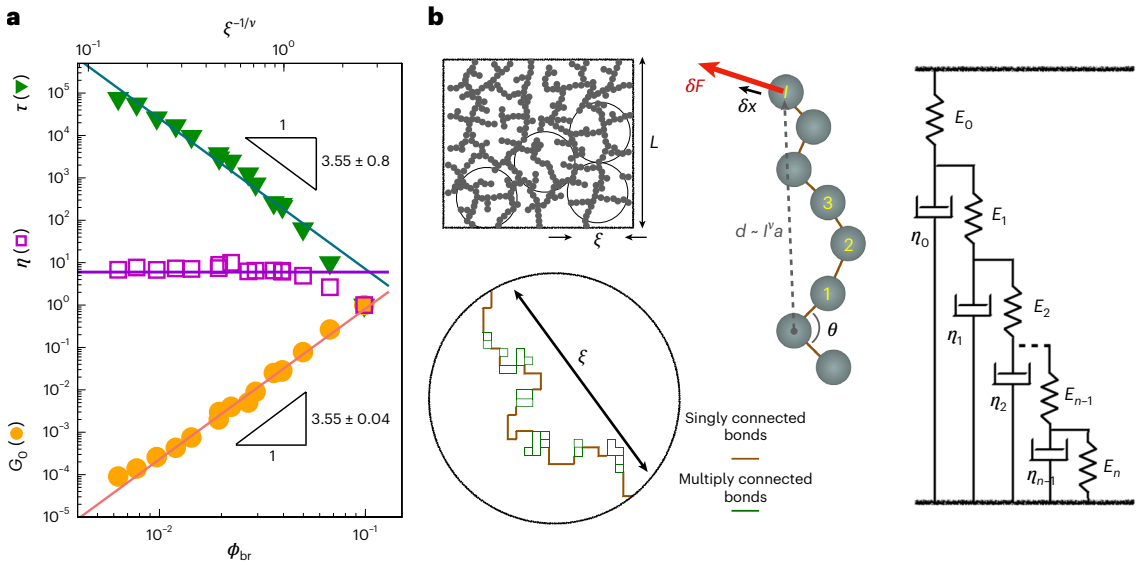

Fig. 4 | Scaling of viscoelastic parameters and connection to the ladder model. a, Scaling of dimensionless retardation time $\tau = a_\phi/\tau_0$ or a_f/τ_0 (triangles), elastic modulus $G_0 = 1/b_\phi$ or $1/b_f$ (circles), made dimensionless using ε/a^3, and the resulting characteristic dimensionless viscosity $\eta = \tau G_0$ (squares) versus volume fraction of branching points ϕ_{br} (bottom axis) and $\xi^{-1/\nu}$ (top axis). Error bars, obtained from sample-to-sample fluctuations, are comparable to the symbol sizes. **b**, Schematic representations of the underlying ladder model: fractal blobs of size given by the correlation length ξ (top left), singly and multiply connected bonds within a single blob (bottom left), bending moment of gel strands for which bond bending costs energy when deformation is applied (middle), and the equivalent hierarchical mechanical element representation, consisting of multiple springs and dashpots (right).

Table 1 | Scaling exponents for the evolution of the gel modulus with $G_0 \propto \phi_{br}^f$ and $G_0 \propto \phi^{f_{obs}}$ for different colloidal aggregation processes

Aggregation process	d_f	f	f_{obs}
DLCA	1.8	3.5	3.6
RLCA	2.1	3.5	4.8
Present work	2.5	3.5	8.1

The observable power-law exponent f_{obs} is related to the power law f by the expression $f_{obs} = f/\nu(d-d_f)$, where $d=3$, $\nu=0.8$ and d_f is the fractal dimension of the gel structure.

for G_0 suggest the following inter-relationship for the number of mechanical elements in each ladder structure:

$$n \propto \left(\frac{L}{a}\right)^{1/2\alpha} N_{SCB}^{(2\nu+1)/2\alpha}. \quad (5)$$

Because each element of linear size $\propto \xi$ implies a number N_{SCB} of singly connected bonds[57], with each pairwise combination of these being a source of bending interactions, we hypothesize that $n \propto N_{SCB}^2$. Combined with equation (5), this constrains the power-law exponent in the ladder model to

$$\alpha = (2\nu + 1)/4. \quad (6)$$

Using $\nu \simeq 0.8$ yields $\alpha = 0.68 \pm 0.1$ for our percolated gels in 3D. The data for tan δ and the corresponding fits from both fractional and ladder models confirm this prediction (Fig. 2b,c).

The product $\eta = G_0\tau$ sets the large-scale rate of dissipation in the gel and is found to be independent of the volume fraction of branching points (Fig. 4a). The viscous dashpot η_0 in the ladder model, which is linked to $\tilde{\eta}_0$, n and η by equations (1) and (4), therefore follows the scaling

$$\eta_0 \propto \left(\frac{L}{a}\right)^{d-3+1/\alpha} N_{SCB}^{\nu d-3} \eta, \quad (7)$$

where η can also be directly connected to the drag coefficient ζ in our simulations (Methods). Thus, equation (7) can be understood as a volumetric average measure of the viscous dissipation in a d-dimensional box of size $\propto \xi$ that is filled with N_{SCB} singly connected bonds.

Finally, using equation (1), we can now directly connect the microscopic physics of the gels to the hierarchical organization of the mechanical elements in the ladder model. Indeed, asymptotic expansion of the recursive relations that specify the ladder model (equation (10) in the Methods) produces power-law decays for both the elastic and viscous coefficients as a function of the mode number, that is, we expect $E_i \propto E_0/i^{2\alpha-1}$ and $\eta_i \propto \eta_0/i^{2\alpha-1}$. We show in the following that this hierarchy of internal modes has its origins in the geometrical distribution of effective bending coefficients within the fractal blobs. We first consider the effective bending stiffness that arises from the torsion around the equilibrium angle θ for a certain bond when a force δF is applied on the lth neighbouring bond away from it, along the elastically active backbone of the gel network (see sketch in Fig. 4b). Such an effective bending stiffness decreases by increasing the distance between the bonds along the backbone. As the relative neighbouring distance varies in $1 \le l \le N_{SCB}$, the number of modes in our ladder model varies in the corresponding range $1 \le i \le N_{SCB}^2$, suggesting that $l = i^{1/2}$ is a reasonable mapping between the ith relaxation mode in the ladder model and the portion of a blob constructed from l bonds. We show in the Methods that the effective stiffness for mode $i = l^2$ in the ladder model scales as $k_{i=l^2} = \delta F/\delta x \propto K_0/(l^{2\nu}a^2)$, and that the equivalent spring modulus of the ith mode is $E_{i=l^2} \propto (K_0/a^3)/l^{2\nu-1} = (K_0/a^3)/i^{\nu-1/2}$. An identical power-law decay in fact appears in the corresponding scaling for the viscous model parameters and one can clearly identify $(E_i, \eta_i) = (1/i^{\nu-1/2})(E_0, \eta_0)$. Using equation (6), these two power-law decays simplify to $(E_i, \eta_i) = (1/i^{2\alpha-1})(E_0, \eta_0)$, which, remarkably, corresponds to the recursive relationship required in the ladder model to produce a power-law rheological response. These results demonstrate that the geometrical, self-similar arrangement of singly connected bonds and the cooperative dynamics of bending interactions within individual fractal blobs lie jointly at the origin of the hierarchical order of the corresponding ladder-based/fractional models that compactly and

effectively capture the power-law response of different colloidal gels over a wide range of timescales. On this basis, the viscoelastic master curve becomes a discriminating probe of the proximity to the rigidity threshold and of the marginal stability of particulate gels.

The fractal units and hierarchy of connectivities embedded in soft particulate gels may be buried in the static microstructure (clusters, strands, meshes, and so on) that is directly accessible through confocal imaging or scattering, but they are revealed by measurements of linear viscoelasticity because these hidden structures govern stress transmission and elasticity. As such, they are naturally akin to force chains in granular media or localized excitations arising in amorphous solids[59,60], and their spatial organization potentially determines the hierarchical stress transmission and redistribution under load, from particles to clusters and strands[61–63]. The ideas presented here show how mechanical spectroscopy can be used to understand the emergent viscoelastic properties of a broad range of technologically relevant materials, providing insight across a broad experimental literature and a new scientific basis for material design in areas from 3D printing to recycling. Future work, in fact, can build on this study to investigate the implications of fractal characteristics and hierarchical organization of particulate gels for nonlinear properties, memory encoding and smart adaptive response of soft materials.

Online content

Any methods, additional references, Nature Portfolio reporting summaries, source data, extended data, supplementary information, acknowledgements, peer review information; details of author contributions and competing interests; and statements of data and code availability are available at https://doi.org/10.1038/s41567-023-01988-7.

References

1. Flory, P. J. *Principles of Polymer Chemistry* (Cornell Univ. Press, 1954).
2. de Gennes, P. G. *Scaling Concepts in Polymer Physics* (Cornell Univ. Press, 1979).
3. Stauffer, D., Coniglio, A. & Adam, M. in *Gelation and Critical Phenomena* (ed Dušek, K.) 103–158 (Springer, 1982).
4. Daoud, M. Viscoelasticity near the sol-gel transition. *Macromolecules* **33**, 3019–3022 (2000).
5. Winter, H. H. & Chambon, F. Analysis of linear viscoelasticity of a crosslinking polymer at the gel point. *J. Rheol.* **30**, 367–382 (1986).
6. Muthukumar, M. Screening effect on viscoelasticity near the gel point. *Macromolecules* **22**, 4656–4658 (1989).
7. Martin, J. E., Adolf, D. & Wilcoxon, J. P. Viscoelasticity of near-critical gels. *Phys. Rev. Lett.* **61**, 2620–2623 (1988).
8. Adolf, D., Martin, J. E. & Wilcoxon, J. P. Evolution of structure and viscoelasticity in an epoxy near the sol-gel transition. *Macromolecules* **23**, 527–531 (1990).
9. Witten, T. A. & Pincus, P. *Structured Fluids* (Oxford Univ. Press, 2004).
10. Trappe, V., Prasad, V., Cipelletti, L., Segre, P. N. & Weitz, D. A. Jamming phase diagram for attractive particles. *Nature* **411**, 772–775 (2001).
11. Lu, P. J. et al. Gelation of particles with short-range attraction. *Nature* **453**, 499–503 (2008).
12. Petekidis, G. & Wagner, N. J. in *Rheology of Colloidal Glasses and Gels* (eds Wagner, N. J. & Mewis, J.) 173–226 (Cambridge Univ. Press, 2021).
13. Royall, C. P., Faers, M. A., Fussell, S. L. & Hallett, J. E. Real space analysis of colloidal gels: triumphs, challenges and future directions. *J. Condens. Matter Phys.* **33**, 453002 (2021).
14. Zhang, S. et al. Correlated rigidity percolation and colloidal gels. *Phys. Rev. Lett.* **123**, 058001 (2019).
15. Whitaker, K. A. et al. Colloidal gel elasticity arises from the packing of locally glassy clusters. *Nat. Commun.* **10**, 2237 (2019).
16. Tsurusawa, H., Leocmach, M., Russo, J. & Tanaka, H. Direct link between mechanical stability in gels and percolation of isostatic particles. *Sci. Adv.* **5**, eaav6090 (2019).
17. Dinsmore, A. D. & Weitz, D. A. Direct imaging of three-dimensional structure and topology of colloidal gels. *J. Phys. Condens. Matter* **14**, 7581–7597 (2002).
18. Duri, A. & Cipelletti, L. Length scale dependence of dynamical heterogeneity in a colloidal fractal gel. *Europhys. Lett.* **76**, 972–978 (2006).
19. Szakasits, M. E., Zhang, W. & Solomon, M. J. Dynamics of fractal cluster gels with embedded active colloids. *Phys. Rev. Lett.* **119**, 058001 (2017).
20. Negi, A. S., Redmon, C. G., Ramakrishnan, S. & Osuji, C. O. Viscoelasticity of a colloidal gel during dynamical arrest: evolution through the critical gel and comparison with a soft colloidal glass. *J. Rheol.* **58**, 1557–1579 (2014).
21. Aime, S., Cipelletti, L. & Ramos, L. Power law viscoelasticity of a fractal colloidal gel. *J. Rheol.* **62**, 1429–1441 (2018).
22. Keshavarz, B. et al. Time-connectivity superposition and the gel/glass duality of weak colloidal gels. *Proc. Natl Acad. Sci. USA* **118**, e2022339118 (2021).
23. Shih, W.-H., Shih, W. Y., Kim, S.-I., Liu, J. & Aksay, I. A. Scaling behavior of the elastic properties of colloidal gels. *Phys. Rev. A* **42**, 4772–4779 (1990).
24. Buscall, R., Mills, P. D. A., Goodwin, J. W. & Lawson, D. W. Scaling behaviour of the rheology of aggregate networks formed from colloidal particles. *J. Chem. Soc. Faraday Trans. 1* **84**, 4249–4260 (1988).
25. Grant, M. C. & Russel, W. B. Volume-fraction dependence of elastic moduli and transition temperatures for colloidal silica gels. *Phys. Rev. E* **47**, 2606–2614 (1993).
26. Piau, J.-M., Dorget, M., Palierne, J.-F. & Pouchelon, A. Shear elasticity and yield stress of silica-silicone physical gels: fractal approach. *J. Rheol.* **43**, 305–314 (1999).
27. Trappe, V. & Weitz, D. A. Scaling of the viscoelasticity of weakly attractive particles. *Phys. Rev. Lett.* **85**, 449–452 (2000).
28. Prasad, V. et al. Rideal lecture universal features of the fluid to solid transition for attractive colloidal particles. *Faraday Discuss.* **123**, 1–12 (2003).
29. Wyss, H. M., Deliormanli, A. M., Tervoort, E. & Gauckler, L. J. Influence of microstructure on the rheological behavior of dense particle gels. *AIChE J.* **51**, 134–141 (2005).
30. Yanez, J. A., Shikata, T., Lange, F. F. & Pearson, D. S. Shear modulus and yield stress measurements of attractive alumina particle networks in aqueous slurries. *J. Am. Ceram. Soc.* **79**, 2917–2917 (1996).
31. Ramakrishnan, S., Chen, Y.-L., Schweizer, K. S. & Zukoski, C. F. Elasticity and clustering in concentrated depletion gels. *Phys. Rev. E* **70**, 040401 (2004).
32. Mellema, M., van Opheusden, J. H. J. & van Vliet, T. Categorization of rheological scaling models for particle gels applied to casein gels. *J. Rheol.* **46**, 11–29 (2002).
33. Romer, S., Bissig, H., Schurtenberger, P. & Scheffold, F. Rheology and internal dynamics of colloidal gels from the dilute to the concentrated regime. *Europhys. Lett.* **108**, 48006 (2014).
34. Colombo, J. & Del Gado, E. Self-assembly and cooperative dynamics of a model colloidal gel network. *Soft Matter* **10**, 4003–4015 (2014).
35. Colombo, J. & Del Gado, E. Stress localization, stiffening and yielding in a model colloidal gel. *J. Rheol.* **58**, 1089–1116 (2014).
36. Bouzid, M., Colombo, J., Barbosa, L. V. & Del Gado, E. Elastically driven intermittent microscopic dynamics in soft solids. *Nat. Commun.* **8**, 15846 (2017).

37. Bouzid, M. et al. Computing the linear viscoelastic properties of soft gels using an optimally windowed chirp protocol. *J. Rheol.* **62**, 1037–1050 (2018).
38. Bantawa, M., Fontaine-Seiler, W. A., Olmsted, P. D. & Del Gado, E. Microscopic interactions and emerging elasticity in model soft particulate gels. *J. Phys. Condens. Matter* **33**, 414001 (2021).
39. Geri, M. et al. Time-resolved mechanical spectroscopy of soft materials via optimally windowed chirps. *Phys. Rev. X* **8**, 041042 (2018).
40. Helgeson, M. E. et al. Homogeneous percolation versus arrested phase separation in attractively-driven nanoemulsion colloidal gels. *Soft Matter* **10**, 3122–3133 (2014).
41. Rao, A., Divoux, T., McKinley, G. H. & Hart, A. J. Shear melting and recovery of crosslinkable cellulose nanocrystal-polymer gels. *Soft Matter* **15**, 4401–4412 (2019).
42. Huang, S.-T., Yang, C.-H., Lin, P.-J., Su, C. Y. & Hua, C.-C. Multiscale structural and rheological features of colloidal low-methoxyl pectin solutions and calcium-induced sol-gel transition. *Phys. Chem. Chem. Phys.* **23**, 19269–19279 (2021).
43. Schiessel, H. & Blumen, A. Hierarchical analogues to fractional relaxation equations. *J. Phys. A Math. Theor.* **26**, 5057–5069 (1993).
44. Schiessel, H. & Blumen, A. Mesoscopic pictures of the sol-gel transition: ladder models and fractal networks. *Macromolecules* **28**, 4013–4019 (1995).
45. Jaishankar, A. & McKinley, G. H. Power-law rheology in the bulk and at the interface: quasi-properties and fractional constitutive equations. *Proc. R. Soc. A Math. Phys. Eng. Sci.* **469**, 20120284 (2013).
46. De Gennes, P. G. Coil-stretch transition of dilute flexible polymers under ultrahigh velocity gradients. *J. Chem. Phys.* **60**, 5030–5042 (1974).
47. Stauffer, D. Gelation in concentrated critically branched polymer solutions. Percolation scaling theory of intramolecular bond cycles. *J. Chem. Soc. Faraday Trans. 2* **72**, 1354–1364 (1976).
48. Stauffer, D. & Aharony, A. *Introduction to Percolation Theory* (CRC Press, 2018).
49. Colombo, J., Widmer-Cooper, A. & Del Gado, E. Microscopic picture of cooperative processes in restructuring gel networks. *Phys. Rev. Lett.* **110**, 198301 (2013).
50. Bouzid, M. & Del Gado, E. Network topology in soft gels: hardening and softening materials. *Langmuir* **34**, 773–781 (2018).
51. Shivers, J., Arzash, S., Sharma, A. & MacKintosh, F. C. Scaling theory for mechanical critical behavior in fiber networks. *Phys. Rev. Lett.* **122**, 188003 (2019).
52. Burla, F., Mulla, Y., Vos, B. E., Aufderhorst-Roberts, A. & Koenderink, G. H. From mechanical resilience to active material properties in biopolymer networks. *Nat. Rev. Phys.* **1**, 249–263 (2019).
53. Rocklin, D. Z., Hsiao, L., Szakasits, M., Solomon, M. J. & Mao, X. Elasticity of colloidal gels: structural heterogeneity, floppy modes and rigidity. *Soft Matter* **17**, 6929–6934 (2021).
54. Coniglio, A. Thermal phase transition of the dilute s-state Potts and *n*-vector models at the percolation threshold. *Phys. Rev. Lett.* **46**, 250–253 (1981).
55. Lin, M. Y. et al. Universality of fractal aggregates as probed by light scattering. *Proc. R. Soc. A Math. Phys. Eng. Sci.* **423**, 71–87 (1989).
56. Weitz, D. A., Huang, J. S., Lin, M. Y. & Sung, J. Limits of the fractal dimension for irreversible kinetic aggregation of gold colloids. *Phys. Rev. Lett.* **54**, 1416–1419 (1985).
57. Kantor, Y. & Webman, I. Elastic properties of random percolating systems. *Phys. Rev. Lett.* **52**, 1891–1894 (1984).
58. Grant, M. C. & Russel, W. B. Volume-fraction dependence of elastic moduli and transition temperatures for colloidal silica gels. *Phys. Rev. E* **47**, 2606–2614 (1993).
59. Cates, M. E., Wittmer, J. P., Bouchaud, J.-P. & Claudin, P. Jamming, force chains and fragile matter. *Phys. Rev. Lett.* **81**, 1841–1844 (1998).
60. Nampoothiri, J. N. et al. Emergent elasticity in amorphous solids. *Phys. Rev. Lett.* **125**, 118002 (2020).
61. Hsiao, L. C., Newman, R. S., Glotzer, S. C. & Solomon, M. J. Role of isostaticity and load-bearing microstructure in the elasticity of yielded colloidal gels. *Proc. Natl Acad. Sci. USA* **109**, 16029–16034 (2012).
62. Lindstrom, S. B., Kodger, T. E., Sprakel, J. & Weitz, D. A. Structures, stresses, and fluctuations in the delayed failure of colloidal gels. *Soft Matter* **8**, 3657–3664 (2012).
63. van Doorn, J. M., Verweij, J. E., Sprakel, J. & van der Gucht, J. Strand plasticity governs fatigue in colloidal gels. *Phys. Rev. Lett.* **120**, 208005 (2018).

Methods

Numerical model and simulation

In the simulations, colloidal particles or aggregates, described as spherical objects of diameter a, spontaneously self-assemble into a gel network due to attractive short-range interactions[64] of maximum strength ε, mediated by the solvent in which they are immersed and through which their thermal motion is overdamped. In real particulate gels, surface roughness, shape irregularity and sintering processes limit the relative motion of particles as they aggregate[15,17,65]. These effects are included in the model through an angular modulation of the net attraction that introduces a bending rigidity of the interparticle bonds[38]. Each gel is characterized by its solid volume fraction, estimated as $\phi = (\pi/6)Na^3/L^3$, with N being the total number of particles and L the linear size of the cubic simulation box. For each value of ϕ, various gel microstructures are obtained by tuning the rate Γ at which the relative strength of the attractive interactions (with respect to k_BT) is increased to induce gelation during the sample preparation. For the set of model parameters used here, all networks start from one-particle-thick semi-flexible strands (where particles have coordination number $z = 2$) that branch ($z = 3$) to reduce steric hindrances and frustration as they grow from different directions. Starting from these relatively simplified structural units, however, large-scale numerical simulations (>10^5 colloidal units) allow for hierarchical loops and larger-scale heterogeneities to naturally emerge during the gel self-assembly, depending on the gelation rate. As a consequence, the resulting disordered and heterogeneous network topologies are representative, at a coarse-grained level, of the structural complexity typical of a wide range of soft particulate gels[15,16,65,66].

For all ϕ and Γ considered here, any further aging of the gels beyond the gel preparation is much slower than the simulation time window used to compute the rheological response of the samples, so it can be considered negligible in the context of this study. We use samples with N varying between 2×10^3 and 2×10^5, and L varying from 23 to 120 particle diameters. Γ is varied between $10^{-3}\,\varepsilon/k_B\tau_0$ and $10^{-7}\,\varepsilon/k_B\tau_0$, and the range of particle volume fractions spans $0.05 \le \phi \le 0.15$. In the model, particles interact via a short-range attraction U_2 and a three-body term U_3, which introduces a bending stiffness between neighbouring bonds. Molecular dynamics (MD) simulations with periodic boundaries are implemented for a system of N particles in a cubic box of size L with position vectors $\{\mathbf{r}_1, \ldots, \mathbf{r}_N\}$ and interacting with a potential energy

$$U(\mathbf{r}_1, \ldots, \mathbf{r}_N) = \varepsilon\left[\sum_{i>j} U_2\left(\frac{\mathbf{r}_{ij}}{a}\right) + \sum_i \sum_{j>k}^{j,k\neq i} U_3\left(\frac{\mathbf{r}_{ij}}{a}, \frac{\mathbf{r}_{ik}}{a}\right)\right], \tag{8}$$

where $\mathbf{r}_{ij} = \mathbf{r}_j - \mathbf{r}_i$. The functional forms of U_2 and U_3 are given in Supplementary Section 11 and their detailed description can also be found in previous works[35,38,50]. The MD time unit is expressed in terms of particle mass m, diameter a and unit energy ε as $\tau_{MD} = \sqrt{ma^2/\varepsilon}$. All other physical quantities are measured in units of m, a, ε and τ_{MD}. The equations of motion are solved using a Verlet algorithm with a time step of $\delta t = 0.005\tau_{MD}$. All simulations have been performed using the open-source software LAMMPS[67], modified to incorporate the potential energy (equation (8)). We use statistically independent samples and samples of different sizes to compute sample-to-sample fluctuations and estimate the error bars for the analysis performed.

Gel preparation

The initial gel configurations are prepared by following the protocol described in refs. 35,38. In the following, we briefly summarize the procedure. We use NVT equilibrium MD simulations, with a Nosé–Hoover (NH) thermostat to cool a system of particles in a gas phase initially at a reduced temperature $k_BT_i/\varepsilon = 0.5$ down to $k_BT_f/\varepsilon = 0.05$ in N_{cool} MD steps, which define the cooling (or gelation) rate as $\Gamma = \Delta T/\Delta t = (T_f - T_i)/N_{cool}\delta t$. We verify that the final temperature $k_BT_f/\varepsilon = 0.05$ is low enough for the particles to aggregate and form a percolated gel network. Then, we let the system further equilibrate at $k_BT_f/\varepsilon = 0.05$ with the NH thermostat for additional N_{equi} MD steps. To vary the gelation rate Γ, we change the number of MD steps used for cooling, that is, N_{cool}. The gel configurations are then obtained by draining the kinetic energy from the system. This is carried out by quenching to $k_BT/\varepsilon \approx 0$, using dissipative microscopic dynamics:

$$m\frac{\mathrm{d}^2\mathbf{r}_i}{\mathrm{d}t^2} = -\nabla_{\mathbf{r}_i}U - \zeta\frac{\mathrm{d}\mathbf{r}_i}{\mathrm{d}t}, \tag{9}$$

where ζ is the drag coefficient of the given solvent and we choose $m/\zeta = 1.0\tau_{MD}$. This procedure ensures that the configurations find a local minimum of the potential energy or inherent structure.

The data for varying volume fraction ϕ correspond to a fixed gelation rate of $\Gamma = 10^{-6}\varepsilon/k_B\tau_0$ with $N_{cool} = 10^6$ MD steps and $N_{equi} = 10^6$ MD steps. The data for varying gelation rates Γ correspond to a fixed volume fraction of $\phi = 10\%$, and the gelation rates vary in the range $\Gamma = 10^{-7}\varepsilon/k_B\tau_0$ to $10^{-3}\varepsilon/k_B\tau_0$ with $N_{cool} = 10^8 - 10^4$ MD steps and $N_{equi} = 2 \times 10^4$ MD steps. This variation of gelation rates corresponds to a change in the low-frequency elastic moduli by an order of magnitude (cf. Fig. 1d–f).

Linear viscoelastic spectra

For each gel we use a computational scheme[37] that has been inspired by a recently developed experimental technique[39] and obtain the full linear viscoelastic spectrum by applying an optimally windowed chirp (OWCh) signal. The details of this protocol are presented in Supplementary Section 11. In all linear viscoelastic tests we use an overdamped dynamics with a viscous drag ζ, which introduces a natural time scale $\tau_0 = \zeta a^2/\epsilon = 10\tau_{MD}$, from the balance between the solvent drag and the bond spring. We use this timescale τ_0 as the unit of time throughout.

Master curve for the loss tangent

As demonstrated in Fig. 2a, the viscoelastic spectra of the low-volume-fraction gels, close to the percolation limit, follow the principle of time-connectivity superposition, and the corresponding values of loss tangent will collapse on a master curve for these gels. This simple collapse, which is obtained with just a horizontal shift of the data, is a signature of the self-similarity that exists between the shape of the measured viscoelastic spectra. Thus, we can think of our method in generating a tan δ master curve in Fig. 2a from the measured spectra in Fig. 1g as a general 'discriminating probe' that determines whether the backbone of a mature gel is still similar to the original structure that was formed at the percolation or not.

Mathematical arrangement of model parameters in ladder models

As discussed in refs. 43,44, with simple analysis of continued fractions for ladder models, one can show that the following recursive arrangement is required to obtain a power-law behaviour for the viscoelastic moduli that approaches the critical gel behaviour with exponent α:

$$\begin{aligned}\tilde{E}_i &= \frac{1}{2i-1}\frac{\Gamma(\alpha)}{\Gamma(1-\alpha)}\frac{\Gamma(i+1-\alpha)}{\Gamma(i-1+\alpha)}\tilde{E}_0\\ \tilde{\eta}_i &= 2\frac{\Gamma(\alpha)}{\Gamma(1-\alpha)}\frac{\Gamma(i+1-\alpha)}{\Gamma(i+\alpha)}\tilde{\eta}_0,\end{aligned} \tag{10}$$

where Γ is the complete Gamma function and $1 \le i \le n$ represents the parameter index in the ladder model. This arrangement of parameters leads to a frequency-independent regime for the loss tangent that spans the frequency range $(1/n^2)E_0/\eta_0 \le \omega \le E_0/\eta_0$. For frequencies smaller and larger than the specified span, the ladder model displays asymptotic single-mode retardation and single-mode relaxation consistent with the predictions of the Kelvin–Voigt and Maxwell models, respectively.

By fitting the viscoelastic spectra with the proposed ladder model, one can estimate the number of ladder elements n and develop a quantitative measure for the range of scale-free relaxation modes in a given

gel system. This can be connected to the difference between bounding cutoff lengthscales and timescales in the underlying fractal structure and relaxation spectra of real networks (see Supplementary Section 2 and Supplementary Fig. 2 for further details). Similarly, as shown in equation (10), by determining the power-law exponent α of the ladder or fractional model, we gain extra insight into the mechanical ladder structure's hierarchical arrangement of springs and dashpots.

Microscopic dynamics

The overdamped microscopic dynamics of the gel are probed by using a Langevin dynamics:

$$m\frac{\mathrm{d}^2\mathbf{r}_i}{\mathrm{d}t^2} = -\nabla_{\mathbf{r}_i}U - \zeta\frac{\mathrm{d}\mathbf{r}_i}{\mathrm{d}t} + F_{\mathrm{r}}^i(t), \tag{11}$$

where $m/\zeta = 0.01\tau_0$, and $F_{\mathrm{r}}^i(t)$ is a random white noise that mimics thermal fluctuations and is related to the drag coefficient ζ: $\langle F_{\mathrm{r}}^i(t)F_{\mathrm{r}}^j(t')\rangle = 2\zeta k_{\mathrm{B}}T\delta_{ij}\delta(t-t')$. From the spontaneous particle dynamics with thermal fluctuations $k_{\mathrm{B}}T/\varepsilon = 10^{-3}$ (large enough to induce particle motion but without changing the network topology), we monitor the position of particle i at time t, $\mathbf{r}_i(t) \equiv (x(t), y(t), z(t))$, where x, y and z represent the Cartesian coordinates. The magnitude of the gel displacement is computed as $\Delta_i = ||\mathbf{r}_i(t_0 + t_{\mathrm{w}}) - \mathbf{r}_i(t_0)||$. Both the initial time t_0 and waiting time t_{w} are chosen to be in the plateau of the particle mean-squared displacement curve (Supplementary Fig. 4a) with $t_0 = 10^3\tau_0$ and additional waiting time $t_{\mathrm{w}} = 10^3\tau_0$.

Scaling of physical distance and deformations in the fractal element

Due to the fractal nature of the blobs, the physical distance between neighbours that are l bonds apart is $d \propto al^{\nu}$, and the corresponding torque from force δF scales as $\delta F l^{\nu} a$, which leads to a change of angle $\delta\theta \propto \delta F l^{\nu} a/K_0$. The rotation of this angle leads to a local deformation of $\delta x \propto al^{\nu}\delta\theta$ in the direction of the applied force δF.

Persistence length

The persistence length l_{p} is determined by computing the correlation in the angles of successive bonds along a 50-particle strand sampled over different configurations with the dynamics (equation (11)) at a finite temperature[38]. For the parameters used in this study, the persistence length is estimated to be $l_{\mathrm{p}} \approx 5.5a$.

Data availability

We have deposited the manuscript data in a public repository (https://doi.org/10.5281/zenodo.7580589). Additional data supporting the manuscript data are available from the authors upon request.

Code availability

The codes used in this study are available from the corresponding author upon reasonable request.

References

64. Israelachvili, J. N. *Intermolecular and Surface Forces* (Academic Press, 2015).
65. Dibble, C. J., Kogan, M. & Solomon, M. J. Structural origins of dynamical heterogeneity in colloidal gels. *Phys. Rev. E* **77**, 050401 (2008).
66. Laurati, M. et al. Structure, dynamics and rheology of colloid-polymer mixtures: from liquids to gels. *J. Chem. Phys.* **130**, 134907 (2009).
67. Plimpton, S. Fast parallel algorithms for short-range molecular dynamics. *J. Comput. Phys.* **117**, 1–19 (1995).

Acknowledgements

We acknowledge support from the National Science Foundation, under grants nos. NSF DMR-2026842 (M. Bantawa and E.D.G.) and NSF DMREF CBET—2118962 (E.D.G.). This research was supported in part by the National Science Foundation under grant no. NSF PHY-1748958 through the KITP programme on the Physics of Dense Suspensions.

Author contributions

M. Bantawa and B.K. contributed equally to this work. M. Bantawa performed simulations. B.K. developed the viscoelastic master curve and the rheological ladder model. All authors analysed data and wrote the paper.

Competing interests

The authors declare no competing interests.

Additional information

Supplementary information The online version contains supplementary material available at https://doi.org/10.1038/s41567-023-01988-7.

Correspondence and requests for materials should be addressed to Emanuela Del Gado.

Peer review information *Nature Physics* thanks the anonymous reviewers for their contribution to the peer review of this work.